

# We are IntechOpen, the world's leading publisher of Open Access books Built by scientists, for scientists

6,900

Open access books available

186,000

International authors and editors

200M

Downloads

Our authors are among the

154

Countries delivered to

TOP 1%

most cited scientists

12.2%

Contributors from top 500 universities



WEB OF SCIENCE™

Selection of our books indexed in the Book Citation Index  
in Web of Science™ Core Collection (BKCI)

Interested in publishing with us?  
Contact [book.department@intechopen.com](mailto:book.department@intechopen.com)

Numbers displayed above are based on latest data collected.  
For more information visit [www.intechopen.com](http://www.intechopen.com)



---

# Carbon Nanotube Reinforced Alumina Composite Materials

---

Go Yamamoto and Toshiyuki Hashida

Additional information is available at the end of the chapter

<http://dx.doi.org/10.5772/48667>

---

## 1. Introduction

Novel materials and processing routes provide opportunities for the production of advanced high performance structures for different applications. Ceramic matrix composites are one of these promising materials. Engineering ceramics such as  $\text{Al}_2\text{O}_3$ ,  $\text{Si}_3\text{N}_4$ ,  $\text{SiC}$  and  $\text{ZrO}_2$  produced by conventional manufacturing technology have high stiffness, excellent thermostability and relatively low density, but extreme brittle nature restricted them from many structural applications (Mukerji, 1993). Considerable attention has been adopted to improve the fracture toughness. An approach has been paid to the development of nanocrystalline ceramics with improved fracture properties. Decreasing the grain size of ceramics to the sub- and nano-meter scale leads to a marked increase in fracture strength (Miyahara et al., 1994). However, fracture toughness of nanocrystalline ceramics generally displays modest improvement or even deterioration (Miyahara et al., 1994; Rice, 1996; Yao et al., 2011). As one possible approach, incorporation of particulates, flakes and short/long fibers into ceramics matrix, as a second phase, to produce tougher ceramic materials is an eminent practice for decades (Evans, 1990). Recently, researchers have focused on the carbon nanomaterials, in particular carbon nanotubes (CNTs), which are nanometer-sized tubes of single- (SWCNTs) or multi- layer graphene (MWCNTs) with outstanding mechanical, chemical and electrical properties (Dai et al., 1996; Ebbesen et al., 1996; Treacy et al., 1996; Huang et al., 2006; Peng et al., 2008), motivating their use in ceramic composite materials as a fibrous reinforcing agent.

It is well recognized that some difficulties appear to be the major cause for the limited improvement in CNT/ceramic composites prepared to date. The first is the inhomogeneous dispersion of CNTs in the ceramic matrix. Pristine CNTs are well known for poor solubilization, which leads to phase segregation in the composite owing to the van der Waals attractive force (Chen et al., 1998). Such clustering produces a negative effect on the

physical and mechanical properties of the resultant composites (Yamamoto et al., 2008). The second is the difficulty in controlling connectivity between CNTs and the ceramics matrix, which leads to a limited stress transfer capability from the matrix to the CNTs (Peigney, 2003; Sheldon & Curtin, 2004; Chen et al., 2011). The strengthening and toughening mechanisms of composites by fibers are now well established (Evans, 1990; Hull & Clyne, 1996); central to an understanding is the concept of interaction between the matrix and reinforcing phase during the fracture of the composite. The fracture properties of such composites are dominated by the fiber bridging force resulting from debonding and sliding resistance, which dictates the major contribution to the strength and toughness. Thus, the adequate connectivity with the matrix, and uniform distribution within the matrix are essential structural requirements for the stronger and tougher CNT/ceramic composites. To overcome these obstacles, various efforts, such as surface modification (De Andrade et al., 2008; Yamamoto et al., 2008; Kita et al., 2010; Gonzalez-Julian et al., 2011), heterocoagulation (Fan et al., 2006a, 2006b), extrusion (Peigney et al., 2002), and their combination, have been made to effectively achieve good dispersion of CNTs in ceramic matrix. Until now, however, most results for strengthening and toughening have been disappointing, and only little or no improvement have been reported in CNT/ceramic composite materials, presumably owing to the difficulties in homogeneous dispersion of CNTs in the matrix and in formation of adequate interfacial connectivity between two phases.

This chapter presents that novel processing approach based on the precursor method. The MWCNTs used in this study are modified with an acid treatment. Combined with a mechanical interlock induced by the chemically modified MWCNTs, this approach leads to improved mechanical properties. Mechanical measurements on the composites revealed that only 0.9 vol.% acid-treated MWCNT addition results in 37% and 36% simultaneous increases in bending strength ( $689.6 \pm 29.1$  MPa) and fracture toughness ( $5.90 \pm 0.27$  MPa·m<sup>1/2</sup>), respectively, compared with a MWCNT-free alumina sample prepared under similar processing conditions. Structure-property relationship of present composites will be explained on the basis of the detailed nano/microstructure and fractographic analysis. We also explain why previous reports indicated only modest improvements in the fracture properties of MWCNT based ceramic composites. Here, the failure mechanism of the MWCNTs during crack opening in a MWCNT/alumina composite is investigated through transmission electron microscope (TEM) observations and single nanotube pullout tests. Achieving tougher ceramic composites with MWCNTs is discussed based on these results.

## **2. A novel approach for preparation of MWCNT/alumina composites**

To disperse the MWCNTs homogeneously in the matrix and improve the connectivity between MWCNTs and matrix, we developed a novel approach with combination of a precursor method for synthesis of an alumina matrix, an acid treatment of MWCNTs and a spark plasma sintering method. The improvement on the bending strength and fracture toughness was confirmed by the fracture tests.

## 2.1. Materials and specimen preparation

### 2.1.1. Starting materials

The MWCNT material (Nano Carbon Technologies) used in this research was synthesized by a catalytic chemical vapor deposition method followed by high temperature annealing at 2600°C. The purity was claimed to be 99.5% by the producer. Fig. 1 shows scanning electron microscope (SEM, Hitachi S-4300) and TEM (Hitachi HF-2000) images of the pristine MWCNTs. It can be seen from Fig. 1b that the pristine MWCNTs have a highly crystalline multi-walled structure with a narrow central channel. The corresponding geometrical and mechanical properties of the pristine MWCNT are listed in Table 1. The estimated diameter and length of the pristine MWCNTs from SEM and TEM measurements ranged from 33 to 124 nm (average: 70 nm) and 1.1 to 22.5  $\mu\text{m}$  (average: 8.7  $\mu\text{m}$ ), respectively. Tensile-loading experiments with individual MWCNTs using a nanomanipulator tool operated inside SEM revealed that the tensile strengths of 10 pristine MWCNTs ranged from  $\sim 2$  to  $\sim 48$  GPa (average: 20 GPa) and the Young's modulus ranged from  $\sim 50$  to  $\sim 1360$  GPa (average: 790 GPa) (Yamamoto et al., 2010). It seems that the average tensile strength of the pristine MWCNT used in this research were somewhat lower than that of the arc-discharge grown MWCNTs (Yu et al., 2000).

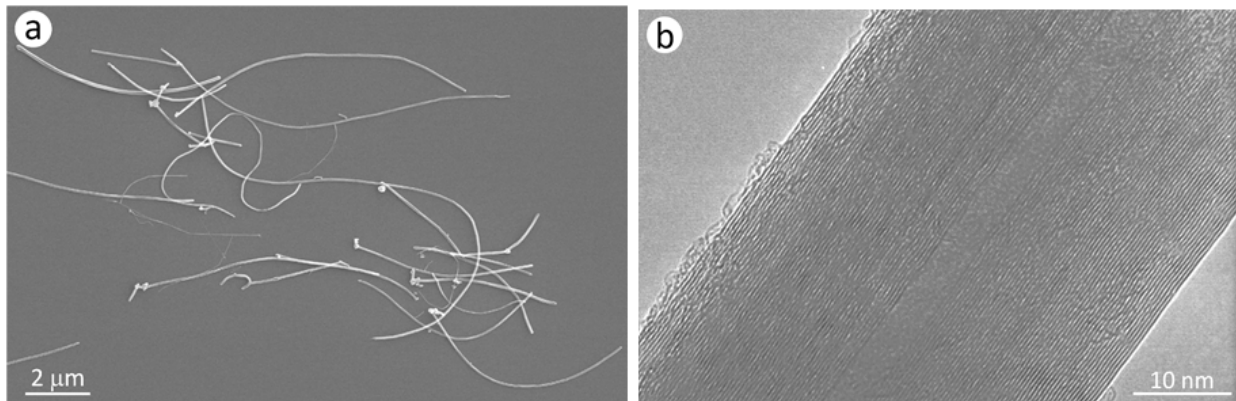


**Figure 1.** (a) SEM and (b) TEM image of pristine MWCNTs used in this research.

ID (nm)	OD (nm)	$l$ ( $\mu\text{m}$ )	$\rho$ ( $\text{Mg}/\text{m}^3$ )	$\sigma_t$ (GPa)	$E$ (GPa)	$I$ ( $\text{nm}^4$ )	$EI$ ( $\text{N}\cdot\text{nm}^2$ )
7 (3~12)	70 (33~124)	8.7 (1.1~22.5)	2.1	20 (2~48)	790 (50~1360)	$1.2 \times 10^6$	$9310 \times 10^{-4}$

**Table 1.** Measured geometrical and mechanical properties of pristine MWCNTs. Shown are the nanotube inner diameter (ID), outer diameter (OD), length ( $l$ ), density ( $\rho$ ), tensile strength ( $\sigma_t$ ), Young's modulus ( $E$ ), moment of inertia of cross sectional area ( $I$ ) and flexural rigidity ( $EI$ ), respectively.

### 2.1.2. Acid treatment of MWCNTs

The rationale behind the acid treatment is to introduce nanoscale defects and adsorb negatively charged functional groups at the MWCNT ends and along their lengths. The

pristine MWCNTs were refluxed in 3:1 (volume ratio) concentrated  $\text{H}_2\text{SO}_4\text{:HNO}_3$  mixture at a temperature of  $70^\circ\text{C}$  for 1 hour, 2 hours and 4 hours, washed thoroughly with distilled water to be acid-free, and then finally dried in an air oven at  $60^\circ\text{C}$ . Fig. 2 shows the typical TEM images of a series of the acid-treated MWCNTs and the corresponding distribution of nanod defect depths treated with the various conditions. It is demonstrated that with the acid treatment of the pristine MWCNTs, we have deliberately introduced nanoscale defects on the surface of the MWCNTs. The depth of the nanod defects is on the nanoscale and the average size is in the range of 4.4–7.0 nm for the acid treatment used in this study. We can see that the nanod defects density, i.e., the number of nanod defects per unit of a MWCNT surface area increases with the increasing treatment time. Hereafter, the number of the nanod defects per unit of the MWCNT surface area is referred to as the nanod defect density.

In addition to the nanod defects density, the average size of the nanod defect depths appears to vary with respect to the treatment time. When the treatment time increases from 1 hour to 2 hours, the average size of nanod defect depths increases from 4.4 nm to 6.5 nm. Furthermore, when the treatment time further increases to 4 hours, it increases to 7.0 nm. The aspect ratio ( $\alpha$ ) of the nanod defects on the MWCNT surface were estimated using the equation  $\alpha = L_{\text{width}}/L_{\text{depth}}$ , where  $L_{\text{width}}$  is the average size of nanod defect widths on the MWCNT surface, and  $L_{\text{depth}}$  is the average size of nanod defect depths. For the acid treated products with treatment time of 1 hour, 2 hours and 4 hours was 4.4, 4.9 and 3.9, respectively. The experimental results demonstrate that the present method, which uses the acid treatment, may provide an effective route for preparation of the nanod defects on the MWCNT surface, and it may be possible to adjust and control the average size and nanod defect density by varying the treatment time. According to the current TEM observations, peel-off of a few layers in the MWCNT structure was frequently observed for the MWCNT powders acid-treated for 4 hours. Thus, reduction of  $\alpha$  may be due to the decrease in the MWCNT diameter by the peel-off of a few layers in the MWCNT structure and imply that the excessive acid treatment of the MWCNT resulted in degradation of the quality and mechanical properties of MWCNTs (Yamamoto et al., 2010). As previously reported (Liu et al., 1998), SWCNTs can be cut into shorter segments by acid treatment of 3:1 (volume ratio) concentrated  $\text{H}_2\text{SO}_4\text{:HNO}_3$  mixture. In this study, however, when the acid treatment times are 1 hour and 2 hours, no such change in the length has been found in the acid-treated MWCNTs. The average lengths of the acid-treated MWCNTs were 8.7  $\mu\text{m}$  and 8.3  $\mu\text{m}$ , respectively. In contrast, average length was decreased slightly with a further increase in the treatment time up to 4 hours, and reached about 7.2  $\mu\text{m}$ .

The zeta potential values of the pristine MWCNTs and the acid-treated MWCNTs at different pH values are shown in Fig. 3a. Here, the changes in zeta potentials were measured in 1.0 mM KCl aqueous solution of varying pH using a zeta potential analyzer (ZEECOM ZC2000, Microtec). The pH value of the aqueous solution was adjusted with HCl and NaOH. Zeta potential values were calculated using the Smoluchowski equation. The isoelectric point ( $\text{pH}_{\text{iep}}$ ) for the pristine MWCNTs is located at about 3.0, whereas the acid

treatment process makes the surface more negatively charged at tested pH values. The change in the zeta potential may be mainly due to the introduction of more functional groups after the acid treatment (Esumi et al., 1996; Liu et al., 1998). These functional groups make them easily dispersed in polar solvents, such as water and ethanol. Fig. 3b shows a photograph of the pristine MWCNTs and acid-treated MWCNTs suspensions at pH 6, respectively. It is clear that the pristine MWCNTs are not dispersed at pH 6. In contrast, the dispersion of the acid-treated MWCNTs is seen to improve dramatically. Furthermore, it can be expected that the larger electrical repulsive force between the acid-treated MWCNTs will facilitate their dispersion and prevent them from tangling and agglomeration. The zeta potential of the aluminum hydroxide, which is used as the starting material for synthesis of the alumina matrix, exhibited positive values over a wide pH range (pH = 3~9), while that of the acid-treated MWCNTs was negative in this pH range. On these two colloidal suspensions are mixed, particles of the aluminum hydroxide will bind onto the acid-treated MWCNTs because of the strong electrostatic attractive force between them, and this results in a homogeneous MWCNTs and aluminum hydroxide solution.

## 2.2. Preparation of MWCNT/alumina composites

A typical synthesis procedure for the composite preparation is as follows. The 50 mg MWCNTs acid-treated for 2 hours or pristine MWCNTs were dispersed in 400 ml ethanol with aid of ultrasonic agitation. 15.2 g aluminum hydroxide (Wako Pure Chemical Industries) was added to this solution and ultrasonically agitated. 73 mg magnesium hydroxide (Wako Pure Chemical Industries) was added to prevent excessive crystal growth. Here, the weight loss of the hydroxides caused by the dehydration process was accounted for in the calculation of the composite composition. The weight loss of the aluminum hydroxide and the magnesium hydroxide was 34.7% and 31.9%, respectively. The resultant suspension was filtered and dried in an air oven at 60°C. Finally, the product obtained in the previous step was put into a half-quartz tube and was dehydrated at 600°C for 15 min in argon atmosphere. The composites were prepared by spark plasma sintering (SPS, SPS-1050 Sumitomo Coal Mining) (Omori, 2000) in a graphite die with an inner diameter of 30 mm at a temperature of 1500°C under a pressure of 20 MPa in vacuum for 10 min. For comparison, similar preparation processes were applied while using the pristine MWCNTs as the starting material. Fig. 4 shows X-ray diffraction patterns (M21Mac Science) of the (a) aluminum hydroxide–MWCNT mixture, (b) dehydrated product and (c) sintered body, respectively. It is difficult to distinguish the MWCNT peaks from all XRD patterns, probably due to the small quantity of MWCNTs. The diffraction peaks corresponding to the aluminum hydroxide and the intermediate were observed in the aluminum hydroxide–MWCNT mixture. However, the diffraction peaks corresponding to the aluminum hydroxide and the intermediate disappeared completely in the sintered body, suggesting the phase transformation of the aluminum hydroxide to form  $\alpha$ -alumina via an amorphous phase (b). These results clearly indicate that alumina was successfully synthesized by SPS at 1500°C under 20 MPa in vacuum.

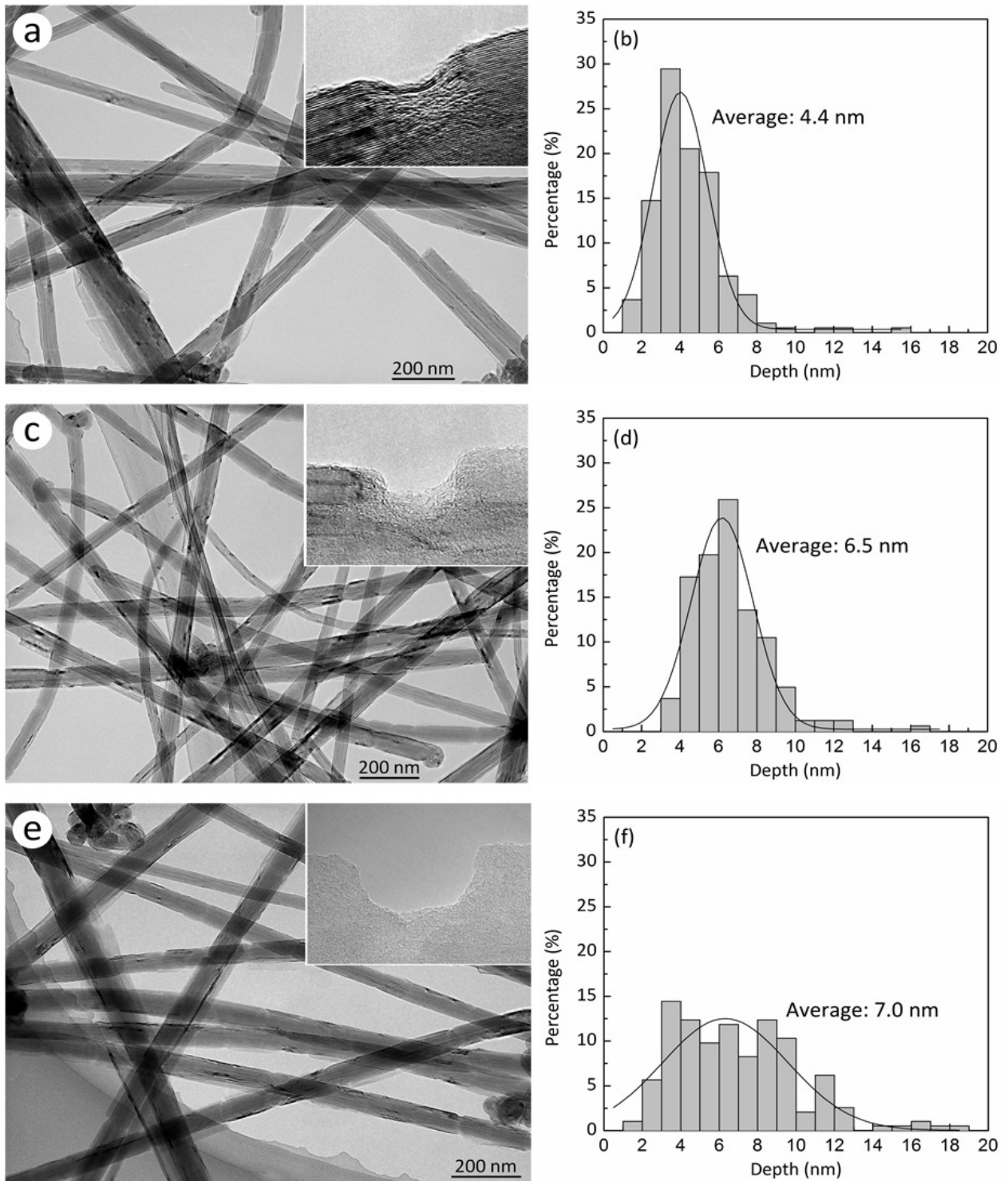


**Figure 2.** Typical low-magnification TEM images of acid-treated MWCNTs treated with the various conditions of (a) 1 hour, (c) 2 hours and (e) 4 hours. The insets show the high magnification images. (b), (d), (f) Corresponding depth distribution of the nanodefeks in the sample (a), (c) and (e), respectively. The solid lines in (b), (d), (f) represent the Gaussian fitting curves. The observation was made for approximately 200 defects.

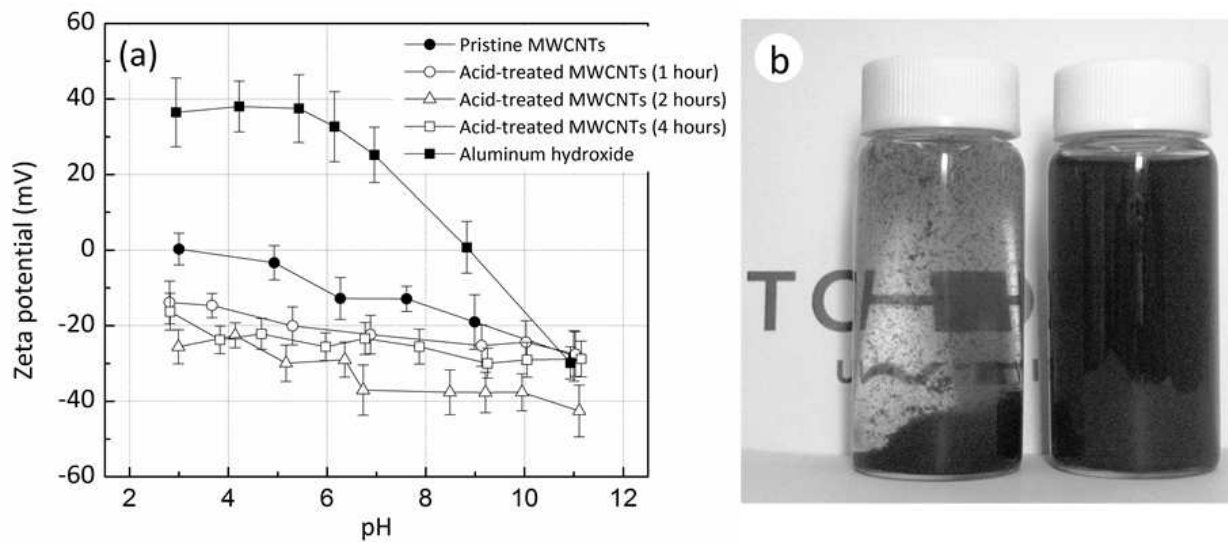


**Figure 3.** (a) Zeta potential values of MWCNTs and acid-treated MWCNTs at different pH. (b) Undistributed one-day old aqueous suspensions of (left) pristine MWCNTs and (right) acid-treated MWCNTs.

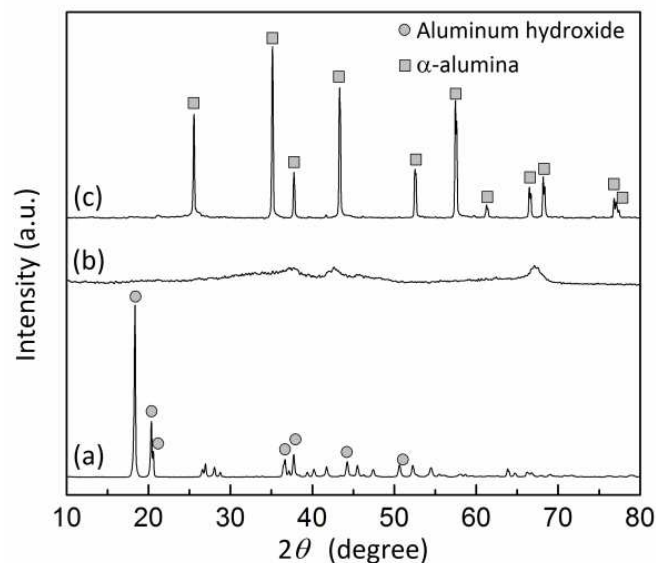


**Figure 4.** XRD patterns of the (a) aluminum hydroxide–MWCNT mixture, (b) dehydrated product and (c) sintered body, respectively.

### 2.3. Micro- and nanostructures of MWCNT/alumina composites

We now discuss the micro- and nanostructures of the acid-treated MWCNT/alumina composites using SEM and TEM analysis. An interesting geometric structure was observed between the individual MWCNT and the alumina matrix, as shown in Fig. 5. It is revealed that a nanodefekt on the acid-treated MWCNT is filled up with alumina crystal, which may be intruding into the nanodefekt during grain growth. This nanostructure is novel in that its structure resembles a nanoscale anchor with an alumina crystal spiking the surface of the MWCNT.

From the SEM observations on the fracture surface, the following features can be noted. First, numerous individual MWCNTs protrude from the fracture surface, and the pullout of the MWCNTs can be clearly observed (Fig. 6a), which had not been obtained until now for conventional CNT/ceramic composites. Most of MWCNTs are located in the intergranular phase and their lengths are in the range 0~10  $\mu\text{m}$ . The alumina grains have sizes in the micron range, around 1.5  $\mu\text{m}$  (The grain size of the composite was obtained using SEM images, and the observation was made for 224 grains.). No clear difference in the grain size is observed between the acid-treated MWCNT/alumina composites and the pristine MWCNT/alumina composites, even though the incorporation of MWCNTs seems to suppress the grain growth of the alumina. Second, in the case of the smaller amount of the acid-treated MWCNTs, no severe phase segregation was observed, whereas the composites made with the pristine MWCNTs revealed an inhomogeneous structure even for MWCNT addition as low as 0.9 vol.%. In addition to the above features, some MWCNTs on the fracture surface showed a "clean break" near the crack plane, and that the diameter of MWCNT drastically slenderized toward their tip, as illustrated in Figs. 6b and 6c, respectively. As SEM cannot clearly resolve the thickness of a single MWCNT, TEM was used to determine if the fracture phenomenon of MWCNTs was indeed occurring during crack opening.

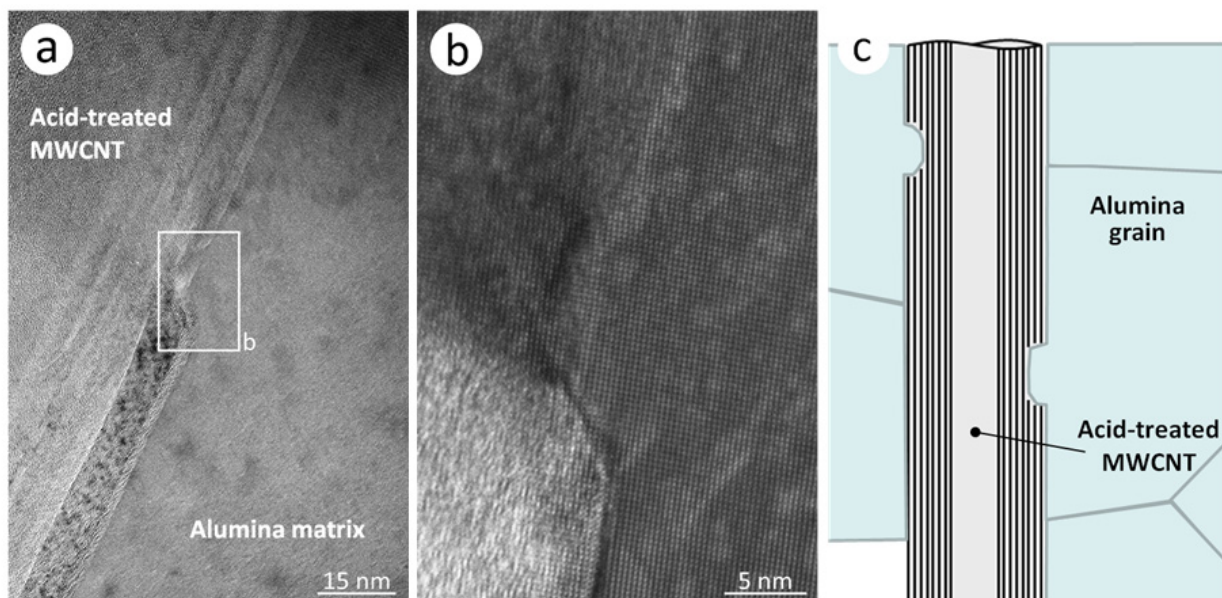


**Figure 5.** MWCNT morphology in the composites. (a) It is demonstrated that a nanodefect on the acid-treated MWCNT is filled up with alumina crystal. (b) Enlarged TEM image, taken from the square area. (c) Schematic description of MWCNT morphology in the composites.

TEM observations on the fracture surface demonstrated that a diameter change in the MWCNT structure was evidently observed for a certain percentage of the MWCNTs (Fig. 7a). At least, 25% MWCNT appear to have an apparent diameter change (The observation was made for 281 MWCNTs.). As shown in Fig. 7b, the high magnification TEM image clearly showed a change in diameter, and this morphology is quite similar to a "sword-in-sheath"-type failure (Yu et al., 2000; Peng et al., 2008; Yamamoto et al., 2010). Key features are illustrated in enlarged TEM image, taken from the square area in Fig. 7b. The inset showed

that outer-walls having approximately 10 shells were observed to break up at the location where the MWCNT undergo failure, and that the edges of the broken outer shells were observed to be perpendicular to the cylinder axis. Since no apparent variation in the diameter of the MWCNTs has been observed along the axis in the as-received MWCNTs, these results imply that some MWCNTs underwent failure in the sword-in-sheath manner prior to pullout from the matrix. Note that MWCNT failure was also observed in fracture surfaces of alumina composites made with arc-discharge-grown and chemical vapor deposition-grown MWCNTs prepared under the same processing conditions (Yamamoto et al., 2011).

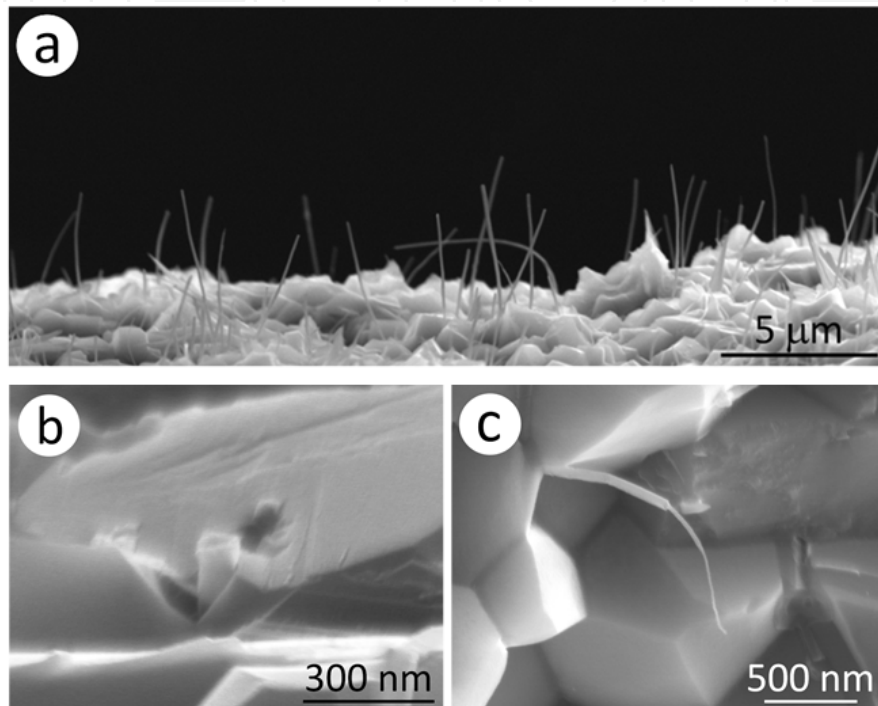


**Figure 6.** Fracture surface of acid-treated MWCNT/alumina composites. (a) Numerous individual MWCNTs protrude from the fracture surface. (b,c) Some MWCNTs have broken in the multi-wall failure.

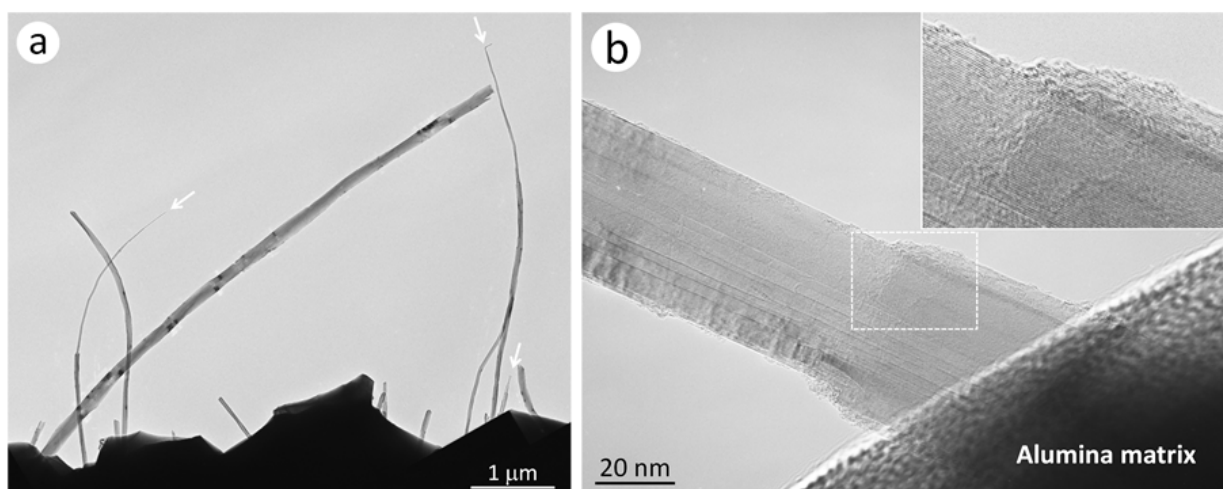


**Figure 7.** TEM images of the fracture surface of the composite acquired (a) low and (b) high magnification images.

## 2.4. Physical and mechanical properties of MWCNT/alumina composites

The bending strength of the composites was measured by the three-point bending method under ambient conditions, in which the size of the test specimens was 2.0 mm (width) × 3.0 mm (thickness) × 24.0 mm (length). The span length and crosshead speed for the strength tests were 20.0 mm and 0.83 μm/s, respectively. The fracture toughness was measured by the single-edge notched beam (SENB) method (Japanese Industrial Standards, 1995) under ambient conditions, in which the size of test specimens was 2.0 mm (width) × 3.0 mm (thickness) × 15.0 mm (length). A notch with depth and width of 0.3 mm and 0.1 mm was cut in the center part of the test specimens. A span length of 12.0 mm and crosshead speed of 0.83 μm/s were applied for the toughness test. The bending strength ( $\sigma_b$ ) and fracture toughness ( $K_{Ic}$ ) are given by the following equations:

$$\sigma_b = 3P_b L / 2bh^2 \quad (1)$$

$$K_{Ic} = \left(3P_b L / 2bh^2\right) \cdot a^{1/2} \gamma \quad (2)$$

where  $P_b$  is the maximum load,  $L$  is the span length,  $b$  is the specimen width,  $h$  is the specimen thickness,  $a$  is the notch depth and  $\gamma$  is the dimensional factor. All surfaces of the specimens were finely ground on a diamond wheel, and the edges were chamfered. The indentation tests were done on a hardness tester (AVK-A, Akashi) with a diamond Vickers indenter under ambient conditions. The 0.9 vol.% acid-treated MWCNT/alumina composite with surface roughness of 0.1 μm ( $R_a$ ) was indented using a Vickers diamond pyramid with a load of 98.1 N ( $P$ ) applied on the surface for 15 s. The diagonal ( $d$ ) and the radial crack length ( $C$ ) were measured by the SEM. The hardness ( $Hv$ ) and indentation toughness values ( $K_{Ic}$ ) were calculated by the following equations:

$$Hv = 0.1891P / d^2 \quad (3)$$

$$K_{Ic} = 0.016(E / H_v)^{1/2} (P / C^{3/2}) \quad (4)$$

where  $E$  is the Young's modulus of the composite ( $E = 362.8$  GPa) measured by a pulse-echo method.

It was found that surface modification of the MWCNTs is effective in improvement of bending strength and fracture toughness of the MWCNT/alumina composites. Figs. 8a and 8b show the dependence of the bending strength and the fracture toughness on MWCNT content in the composites. There are few papers which report significant improvement in the mechanical properties such as toughness (Zhan et al., 2003), and the improvement by MWCNT addition has been limited so far in previous studies (Ma et al., 1998; Sun et al., 2002; Wang et al., 2004; Sun et al., 2005; Cho et al., 2009). In our composites, however, the bending strength and the fracture toughness simultaneously increased with the addition of

a small amount of the acid-treated MWCNTs. The bending strength and the fracture toughness of the 0.9 vol.% acid-treated MWCNT/alumina composite reached  $689.6 \pm 29.1$  MPa and  $5.90 \pm 0.27$  MPa·m<sup>1/2</sup>, respectively. At the same time, the bending strength and the fracture toughness of the acid-treated MWCNT/alumina composites were always higher than those of the pristine MWCNT/alumina composites with identical MWCNT content, indicating enhanced stress transfer capability from the alumina to the acid-treated MWCNTs. The Vickers indentation toughness calculated by using the Eq. (4) was 6.64 MPa·m<sup>1/2</sup>, which is a slightly larger value than that measured by using SENB method (5.90 MPa·m<sup>1/2</sup>). These observations revealed that the high structural homogeneity and enhanced frictional resistance of the structural components led to a simultaneous increase in the strength and the toughness of the acid-treated MWCNT/alumina composites. In contrast, for the larger amount of the MWCNTs, the degradation of mechanical properties of both the composites may be primarily attributed to the severe phase segregation. Because a bundle of segregated CNTs has poor load-carrying ability, the effect of this kind of CNT aggregate in the matrix may be similar to that of pores (Yamamoto et al., 2008a, 2008b).

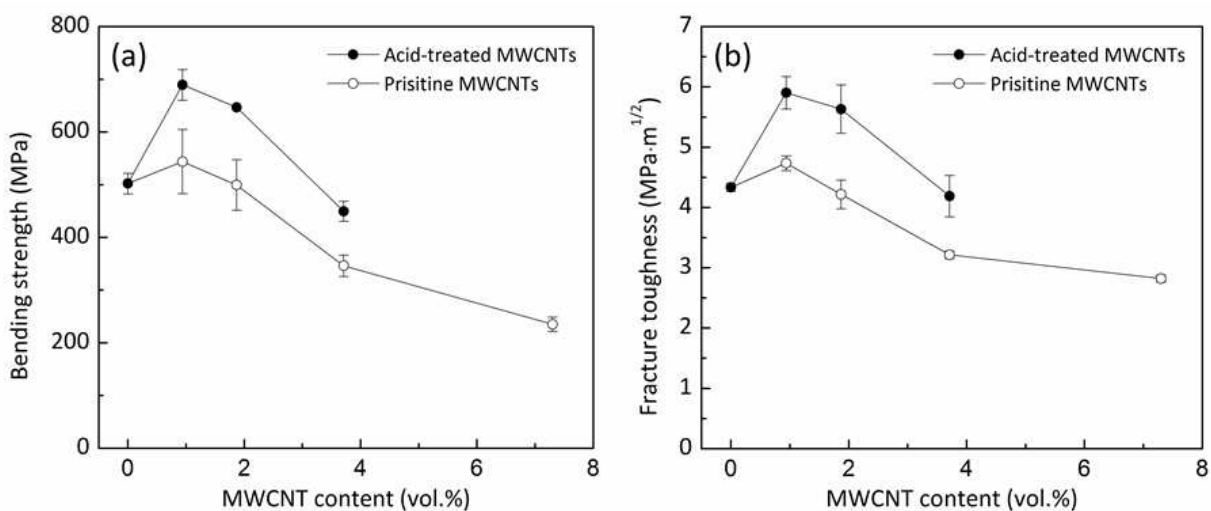


**Figure 8.** (a) Bending strength and (b) fracture toughness as a function of MWCNT content.

### 3. Evaluation of crack bridging characteristics

Ceramic-CNT interfacial behavior is another key factor in controlling the mechanical and physical properties of fiber reinforced composite materials (Evans, 1990; Hull & Clyne, 1996; Chen et al., 2011). In general, strong interfacial connectivity facilitates effective load transfer effect, but it prevents CNT pull-out toughening from occurring. Weak interfacial connectivity favors CNTs pull-out but fails to toughen the ceramic matrix. Thus, a balance must be maintained between CNT pull-out and toughening mechanics. It is well recognized that improved toughness of fiber-reinforced ceramic composites is obtained under moderate fiber-ceramic interfacial connectivity. In this regard, suitable (neither too strong nor too weak) ceramic-CNT interfacial connectivity is needed to ensure effective load transfer, and to enhance the toughness and strength of ceramic-CNT composites.

Here, the failure mechanism of the MWCNTs during crack opening in a MWCNT/alumina composite is investigated through TEM observations and single nanotube pullout tests. Achieving tougher ceramic composites with MWCNTs is discussed based on these results.

### 3.1. Pullout experiment sample preparation

The MWCNT failure during crack opening motivated our research of the crack bridging characteristics through the single nanotube pullout tests. The single nanotube pullout experiments were carried out using an *in-situ* SEM (Quanta 600 FEG; FEI) method with a nanomanipulator system (Yu et al., 2000; Yamamoto et al., 2010). An atomic force microscope (AFM) cantilever (PPP-ZEILR, nominal force constant 1.6 N/m; NANOSENSORS) was mounted at the end of a piezoelectric bender (ceramic plate bender CMBP01; Noliac) on an X–Y linear motion stage, and the composite with fracture surface (that was coated with platinum) was mounted on an opposing Z linear motion stage. The piezoelectric bender was used to measure the resonant frequency of each cantilever in vacuum. A single MWCNT on the fracture surface was clamped onto a cantilever tip by local electron-beam-induced deposition (EBID) of a carbonaceous material (Ding et al., 2005). As a precursor source for the EBID, we used n-docosane (C<sub>22</sub>H<sub>46</sub>, Alfa Aesar), which was dissolved in toluene to make a 3 mass% solution. A small amount of the solution was dropped on a cut-in-half copper TEM grid. After the solution evaporated, the TEM grid with paraffin source was mounted on the AFM chip, as shown in Fig. 9. The deposition rate of the EBID depends on several factors (Ding et al., 2005). Thus, the amount of the paraffin source, deposition time, and distance between the paraffin source and the cantilever tip were experimentally-optimized. The cantilevers serve as force-sensing elements and the spring constants of each were calculated *in-situ* prior to the pullout test using the resonance method (Sader et al., 1999). In brief, for the case of a rectangular cantilever, the force constant ( $k$ ) is given by following equation,

$$k = M_e \rho_c b h L \omega_{vac}^2 \quad (5)$$

where  $\omega_{vac}$  is the fundamental radial resonant frequency of the cantilever in vacuum,  $h$ ,  $b$ , and  $L$  are the thickness, width, and length of the cantilever, respectively,  $\rho_c$  is the density of the cantilever ( $= 2.33 \text{ Mg/m}^3$ ), and  $M_e$  is the normalized effective mass which takes the value  $M_e = 0.2427$  for  $L/b > 5$  (Sader et al., 1995). We measured  $\omega_{vac}$ ,  $h$ ,  $b$  and  $L$  of each cantilever in the SEM and used the measured, not the nominal provided, values to calculate  $k$ . The  $h$ ,  $b$  and  $L$  are determined by counting the number of pixels in the acquired SEM images. The applied force is calculated from the angle of deflection at the cantilever tip in the acquired SEM images (Ding et al., 2006). The deflection ( $\delta$ ) and angle of deflection ( $\theta$ ) at the cantilever tip are given by

$$\delta = PL^3 / 3EI \quad (6)$$

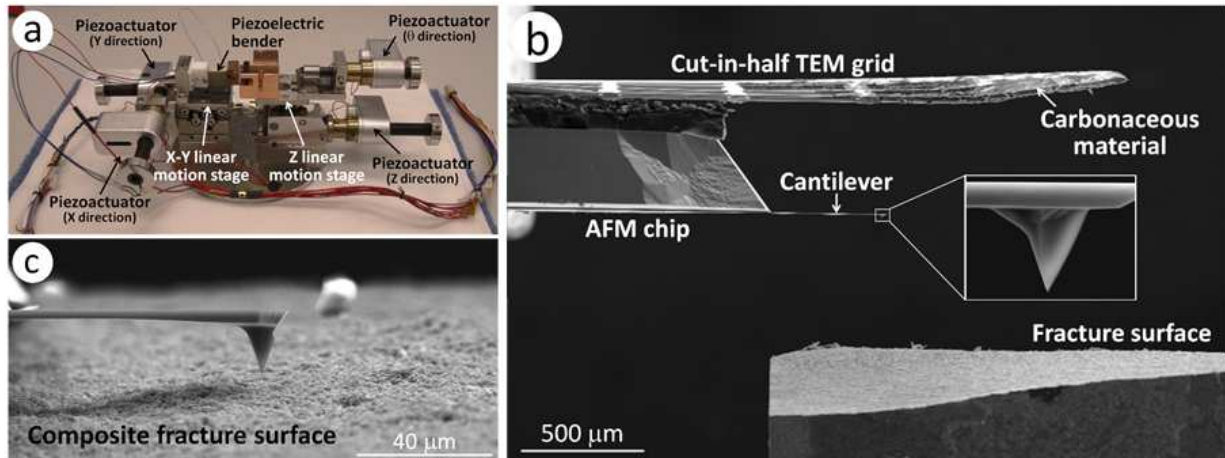


**Figure 9.** SEM image showing the experimental setup for pullout experiments.

$$\theta = PL^2 / 2EI \quad (7)$$

where  $P$  is the load applied at the cantilever tip,  $L$  is the cantilever length,  $E$  is the elastic modulus and  $I$  is the moment of inertia of the cantilever (Ding et al., 2006). Thus, the deflection at the cantilever tip can be represented by the angle of deflection with the following relationship (Ding et al., 2006):

$$\delta = 2\theta L / 3 \quad (8)$$

A crosshead speed – i.e., movement rate of the cantilever – of about 100 nm/s was applied for the pullout tests.

We fractured a composite specimen by conducting the fracture tests, which caused single MWCNT to project from the crack plane, as exemplified in Fig. 6a. This allows single MWCNT “pickup” with cantilever tip for subsequent tensile loading using the nanomanipulator. As mentioned above, however, the MWCNTs crossing the crack planes were strained during crack opening and possibly underwent failure, as shown in Figs. 6b, 6c and 7. Therefore, by observing the fracture surface on the composites, MWCNTs with no apparent damages were selected for the pullout tests. The physical and mechanical properties, and electrical conductivity of the composite used for the pullout testes are shown in Table 2.

Relative density (%)	Grain size ( $\mu\text{m}$ )	Bending strength (MPa)	Fracture toughness ( $\text{MPa}\cdot\text{m}^{1/2}$ )	Hardness (GPa)	Young's modulus (GPa)	Poisson's ratio
98.9	$1.43\pm 0.31$	$543.8\pm 60.9$	$4.74\pm 0.12$	$17.0 \pm 0.4$	358.0	0.20

**Table 2.** The properties of the composite with 0.9 vol.% pristine MWCNTs. The Young's modulus and Poisson's ratio were measured by the ultrasonic pulse echo method.

### 3.2. Nanotube fracture during the failure of MWCNT/alumina composites

Results obtained from the pullout experiments revealed that strong load transfer was demonstrated, and no pullout behavior was observed for all 15 MWCNTs tested in this present research. Eight of these MWCNTs fractured at the composite surface and the remaining 7 MWCNTs underwent failure in the region between the fixed point on the cantilever and the crack plane, as illustrated in Fig. 10.

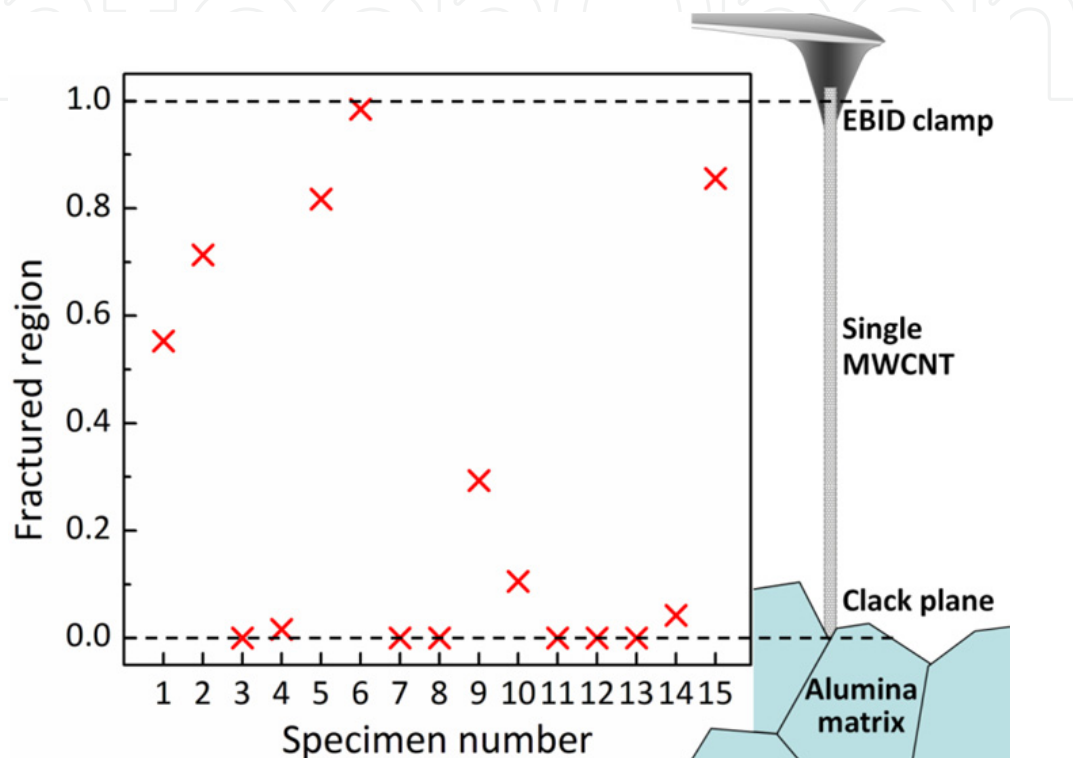


**Figure 10.** Fracture location of single MWCNTs under pullout loading. Of the 15 MWCNTs tested here, 8 MWCNTs fractured on the composite surface (sample numbers: 3, 4, 7, 8, 11–14) and remaining 7 MWCNTs fractured in the middle (sample numbers: 1, 2, 5, 6, 9, 10, and 15).

Two series of SEM and TEM images for each of two individual MWCNTs, captured before and after their breaking, are shown in Figs. 11 and 12. In the first series (Fig. 11; sample number 14), a MWCNT projecting  $5.72 \pm 0.01 \mu\text{m}$  from the fracture surface (Fig. 11a) was "welded" to a cantilever tip by local EBID, and then loaded in increments until failure. The resulting fragment attached on the cantilever tip was at least  $10.9 \mu\text{m}$  long (Fig. 11b), whereas the other fragment remained lodged in a grain boundary of the alumina matrix (Fig. 11c), suggesting that MWCNT underwent failure in a sword-in-sheath manner. TEM images show a change in diameter at the location where the MWCNT underwent failure, and that the inner core protruding from the outer shells has a multi-walled closed-end structure, as shown in Figs. 11d and 11e, respectively. Given that uniformity of the interwall spacing of 0.34-nm-thick cylinder structure, approximately 11 shells underwent failure. These results strongly suggest that the MWCNTs broke in the outer shells and the inner core was then completely pulled away, leaving the companion fragment of the outer shells in the

matrix. The sword-in-sheath failure did not always occur. Instead a few MWCNT failed leaving either a very short sword-in-sheath failure or a clean break. As for one example (Fig. 12; sample number 10), a MWCNT projecting  $5.34 \pm 0.01 \mu\text{m}$  from the crack plane (Fig. 12a) underwent failure on the composite fracture surface. The resulting fragment attached on the cantilever tip was at least  $5.7 \mu\text{m}$  long (Fig. 12b), and no fragment was observed at the original position on the crack plane, suggesting that in this case the MWCNT failed by breaking inside the matrix, and did not pull out. Fig. 12c shows the TEM image of the tip of the same MWCNT which underwent very short sword-in-sheath failure or clean break during crack opening.

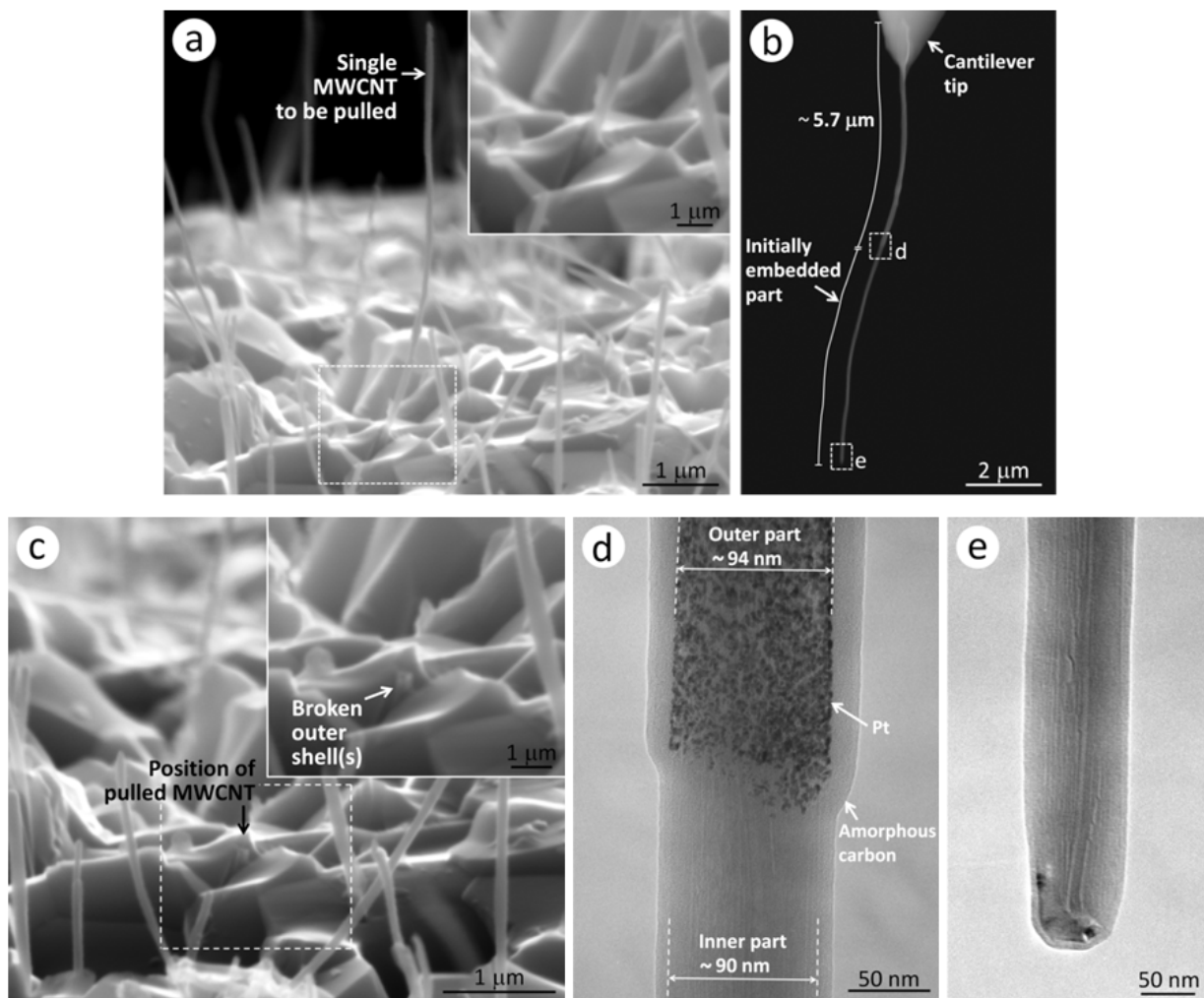


**Figure 11.** SEM images show (a) a free-standing MWCNT having a  $5.72 \pm 0.01 \mu\text{m}$ -long on the fracture surface of the composite. (b) After breaking, one fragment of the same MWCNT attached on the cantilever tip had a length  $\sim 10.9 \mu\text{m}$ . (c) The other fragment remained in the matrix. (d,e) TEM images show a change in diameter at the location where the MWCNT underwent multi-wall failure, and that it clearly has a multi-walled closed-end structure.

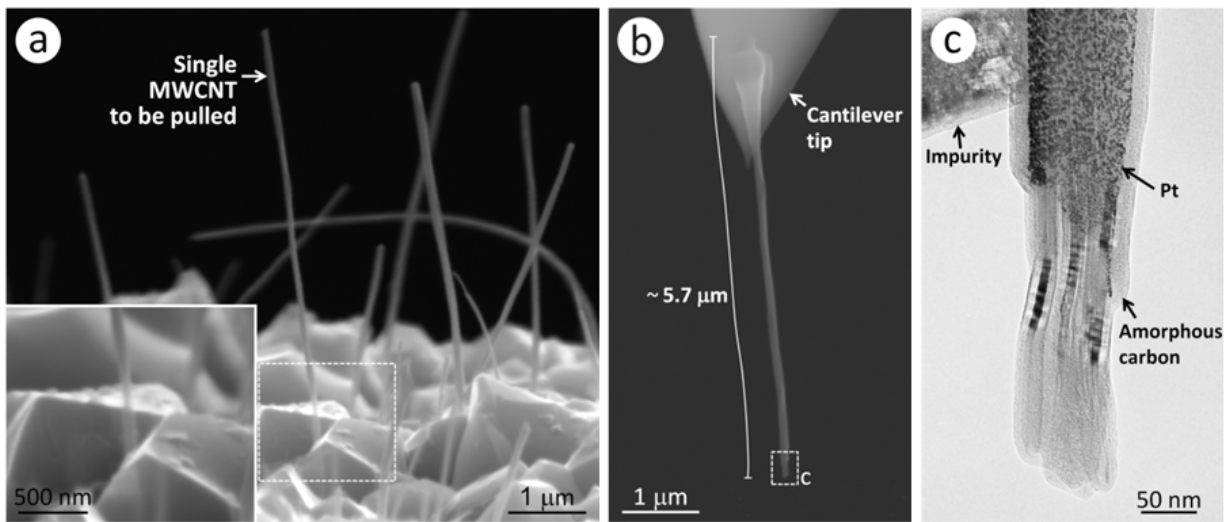


**Figure 12.** In the second series, (a) a tensile-loaded MWCNT with a length of  $4.46 \pm 0.01 \mu\text{m}$  fractured on the crack plane. (b) The resulting fragment on the cantilever tip had a length  $\sim 5.7 \mu\text{m}$ . (c) TEM image shows the MWCNT which underwent the very short sword-in-sheath failure or clean break.

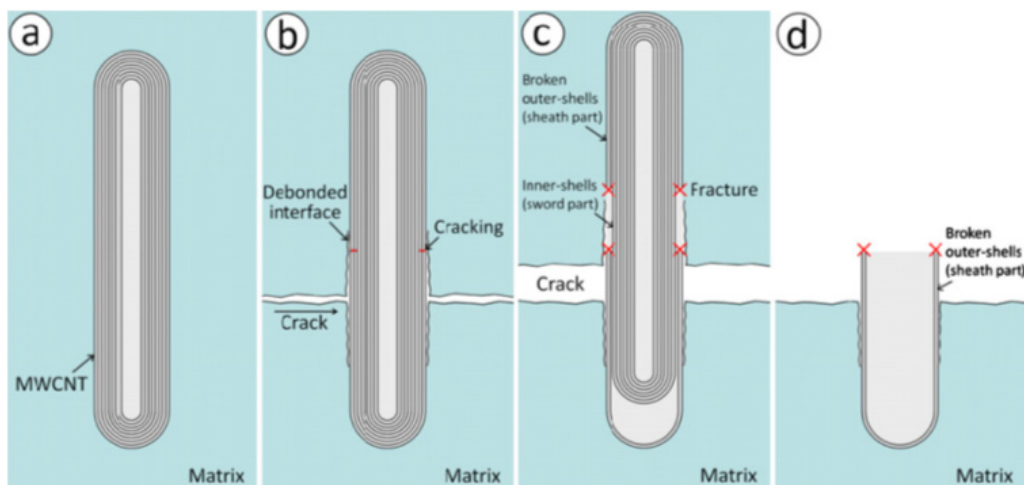


**Figure 13.** Schematic description of possible fracture mechanisms of the MWCNT (sample number 14). (a) Initial state of a MWCNT. (b) Tensile stresses lead to matrix crack and partial debonding formation. (c,d) As displacement increases, the MWCNTs, rather than pulling out from the alumina matrix, undergo failure in the outer shells and the inner core is pulled away, leaving the fragment of the outer shells in the matrix.

Next, we schematically describe possible processes and mechanics, explaining the MWCNT failure during crack opening (Fig. 13). As for one example, considering the sample number 14 (Fig. 11), the initial state of the MWCNT in an ideal case is a completely impregnated and isolated embedded in the matrix (Fig. 13a). Tensile stresses parallel to the axis of MWCNT length lead to matrix crack formation. Subsequently, interfacial debonding between two phases may occur (Fig. 13b), perhaps over a limited distance (but this is unlikely to make a major contribution to the fracture energy.). Since there is variability in the MWCNT strength in the debonded region on either side of the crack plane, and it is possible for the MWCNT to break at a certain position, when the stress in the MWCNT reaches a critical value. As

displacement increases, the MWCNTs, rather than pulling out from the alumina matrix, undergo failure in the outer shells and the inner core is pulled away, leaving the fragments of the outer shells in the matrix (Figs. 13c and 13d).

#### 4. Conclusion

Creating tough, fracture-resistant ceramics has been a central focus of MWCNT/ceramic composites research. In this research, the MWCNT/alumina composite with enhanced mechanical properties of  $689.6 \pm 29.1$  MPa for bending strength and  $5.90 \pm 0.27$  MPa·m<sup>1/2</sup> for fracture toughness have been successfully prepared by a novel processing method. A combination of the precursor method for synthesis of the alumina matrix, the acid treatment of the pristine MWCNTs and the spark plasma sintering method can diminish the phase segregation of MWCNTs, and render MWCNT/alumina composites highly homogeneous. The universality of the method developed here will be applicable to a wide range of functional materials such as tribomaterials, electromagnetic wave absorption materials, electrostrictive materials, and so on. Our present work may give a promising future for the application of MWCNTs in reinforcing structural ceramic components and other materials systems such as polymer- and metal-based composites.

We have also shown from TEM observations and single nanotube pullout experiments on the MWCNT/alumina composites that strong load transfer was revealed, and no MWCNT pullout behavior was observed. It is well recognized the fracture properties of fiber-reinforced composites are dominated by the fiber bridging force resulting from debonding and sliding resistance, which dictates the major contribution to the strength and toughness (Evans, 1990; Hull & Clyne, 1996). The results reported here suggest that modest improvements in toughness reported previously may be due to the way MWCNT's fail during crack opening in the MWCNT/ceramic composites. Our finding suggests important implications for the design of tougher ceramic composites with MWCNTs. The important factor for such tougher ceramic composites will thus be the use of MWCNT having a much higher load carrying capacity (as well as a good dispersion in the matrix).

#### Author details

Go Yamamoto and Toshiyuki Hashida

*Fracture and Reliability Research Institute (FRRI), Tohoku University, Japan*

#### Acknowledgement

The authors thank our colleague, Dr. M. Omori, Mr. K. Shirasu, Mr. Y. Nozaka, Mr. Y. Aizawa and Ms. N. Suzuki of Fracture and Reliability Research Institute (FRRI), Tohoku University, for their helpful discussions, and Mr. T. Miyazaki of Technical Division, School of Engineering, Tohoku University, for technical assistance in the TEM analysis. The authors acknowledge Prof. R.S. Ruoff of The University of Texas at Austin for his useful guidance. This work is partially supported by Grand-in-Aids for Scientific Research (Nos. 23860004

and 21226004) from the Japanese Ministry of Education, Culture, Sports, Science and Technology. This work is performed under the inter-university cooperative research program of the Advanced Research Center of Metallic Glasses, Institute for materials Research, Tohoku University.

## 5. References

- Chen, J.; Hamon, M.A.; Hu, H.; Chen, Y.; Rao, A.M.; Eklund, P.C. & Haddon, R.C. (1998). Solution properties of single-walled carbon nanotubes. *Science*, Vol. 282, pp. 95-98.
- Chen, Y.L.; Liu, B.; Huang, Y.; & Hwang, K.C. (2011). Fracture toughness of carbon nanotube-reinforced metal- and ceramic-matrix composites. *Journal of Nanomaterials*, Vol. 2011, Article ID 746029.
- Cho, J.; Boccaccini, A.R. & Shaffer, M.S.P. (2009). Ceramic matrix composites containing carbon nanotubes. *Journal of Materials Science*, Vol. 44, pp. 1934–1951.
- Dai, H.J.; Wong, E.W. & Lieber, C.M. (1996). Probing electrical transport in nanomaterials: conductivity of individual carbon nanotubes. *Science*, Vol. 272, pp. 523–526.
- De Andrade, M.J.; Lima, M.D.; Bergmann, C.P.; Ramminger, G.D.O.; Balzaretto, N.M.; Costa, T.M.H. & Gallas, M.R. (2008). Carbon nanotube/silica composites obtained by sol-gel and high-pressure techniques. *Nanotechnology*, Vol. 19, article number: 265607.
- Ding, W.; Dikin, D.A.; Chen, X.; Piner, R.D.; Ruoff, R.S.; Zussman, E.; Wang, X. & Li, X. (2005). Mechanics of hydrogenated amorphous carbon deposits from electron-beam-induced deposition of a paraffin precursor. *Journal of Applied Physics*, Vol. 98, article number: 014905.
- Ding, W.Q.; Calabri, L.; Chen, X.Q.; Kohhaas, K.M. & Ruoff, R.S. (2006). Mechanics of crystalline boron nanowires. *Composites Science and Technology*, Vol. 66, pp. 1112–1124.
- Ebbesen, T.W.; Lezec, H.J.; Hiura, H.; Bennett, J.W.; Ghaemi, H.F. & Thio, T. (1996). Electrical conductivity of individual carbon nanotubes. *Nature*, Vol. 382, pp. 54–56.
- Esumi, K.; Ishigami, M.; Nakajima, A.; Sawada, K. & Honda, H. (1996). Chemical treatment of carbon nanotubes. *Carbon*, Vol. 34, pp. 279-281.
- Evans, A.G. (1990) Perspective on the development of high-toughness ceramics. *Journal of the American Ceramic Society*, Vol. 73, pp. 187–206.
- Fan, J.P.; Zhao, D.Q.; Wu, M.S.; Xu, Z. & Song, J. (2006). Preparation and microstructure of multiwalled carbon nanotubes-toughened composite. *Journal of the American Ceramic Society*, Vol. 89, pp. 750–753.
- Fan J.P.; Zhuang, D.M.; Zhao, D.Q.; Zhang, G.; Wu, M.S.; Wei, F. & Fan, Z.J. (2006). Toughening and reinforcing alumina matrix composite with single-wall carbon nanotubes. *Applied Physics Letters*, Vol. 89, pp. 121910-1219103.
- Gonzalez-Julian, J.; Miranzo, P.; Osendi, M.I. & Belmonte, M. (2011). Carbon nanotubes functionalization process for developing ceramic matrix nanocomposites. *Journal of Materials Chemistry*, Vol. 21, pp. 6063-6071.
- Huang, J.Y.; Chen, S.; Wang, Z.Q.; Kempa, K.; Wang, Y.M.; Jo, S.H.; Chen, G.; Dresselhaus, M.S. & Ren, Z.F. (2006). Superplastic carbon nanotubes – conditions have been

- discovered that allow extensive deformation of rigid singlewalled nanotubes. *Nature*, Vol. 439, p. 281.
- Hull, D & Clyne T.W. (1996). *An Introduction to Composite Materials (Second edition)*. Cambridge University Press, 0521388554, The Edinburgh Building, Cambridge CB2 2RU, UK.
- Japanese Industrial Standards (JIS). (1995). R 1607.
- Kita, J.; Suemasu, H.; Davies, I.J.; Koda, S. & Itatani, K. (2010). Fabrication of silicon carbide composites with carbon nanofiber addition and their fracture toughness. *Journal of Materials Science*, Vol. 45, pp. 6052-6058.
- Liu, J.; Rinzler, A.G.; Dai, H.; Hafner, J.H.; Bradley, R.K.; Boul, P.J.; Lu, A.; Iverson, T.; Shelimov, K.; Huffman, C.B.; Rodriguez-Macias, F.; Shon, Y.S.; Lee, T.R.; Colbert, D.T. & Smalley, R.E. (1998). Fullerene pipes. *Science*, Vol. 280, pp. 1253-1256.
- Ma, R.Z.; Wu, J.; Wei, B.Q.; Liang, J. & Wu, D.H. (1998). Processing and properties of carbon nanotubes–nano-SiC ceramic. *Journal of Materials Science*, Vol. 33, pp. 5243-5246.
- Miyahara, N.; Yamaishi, K.; Mutoh, Y.; Uematsu, K. & Inoue, M. (1994). Effects of grain size on strength and fracture toughness in alumina, *JSME International journal* Vol. 37, pp. 231-237.
- Mukerji, J. (1993) Ceramic matrix composites. *Defence Science Journal*, Vol. 43, pp. 385–395.
- Omori, M. (2000). Sintering, consolidation, reaction and crystal growth by the spark plasma system (SPS). *Materials Science and Engineering A*, Vol. 287, pp. 183-188.
- Peigney, A. (2003). Composite materials: tougher ceramics with nanotubes. *Nature Materials*, Vol. 2, pp. 15–16.
- Peigney, A.; Flahaut, E.; Laurent, Ch.; Chastel, F. & Rousset, A. (2002). Aligned carbon nanotubes in ceramics-matrix nanocomposites prepared by high-temperature extrusion. *Chemical Physics Letters*, Vol. 352, pp. 20–25.
- Peng, B.; Locascio, M.; Zapol, P.; Li, S.Y.; Mielke, S.L.; Schatz, G.C. & Espinosa, H.D. (2008). Measurements of near-ultimate strength for multiwalled carbon nanotubes and irradiation-induced crosslinking improvements. *Nature Nanotechnology*, Vol. 3, pp. 626–631.
- Rice, R.W. (1996). Grain size and porosity dependence of ceramic fracture energy and toughness at 22°C, *Journal of Materials Science*, Vol. 31, pp. 1969-1983.
- Sader, J.E.; Chon, J.W.M. & Mulvaney, P. (1999). Calibration of rectangular atomic force microscope cantilevers. *Review of Scientific Instruments*, Vol. 70, pp. 3967–3969.
- Sader, J.E.; Larson, I.; Mulvaney, P. & White, L.R. (1995). Method for the calibration of atomic force microscope cantilevers. *Review of Scientific Instruments*, Vol. 66, pp. 3789-3798.
- Sheldon, B.W. & Curtin, W.A. (2004). Nanoceramic composites: tough to test. *Nature Materials*, Vol. 3, pp. 505–506.
- Sun, L.; Gao, L. & Li, X. (2002). Colloidal processing of carbon nanotube/alumina composites. *Chemistry of Materials*, Vol. 14, pp. 5169–5172.
- Sun, J.; Gao, L. & Xihai Jin, X. (2005). Reinforcement of alumina matrix with multi-walled carbon nanotubes. *Ceramics International*, Vol. 31, pp. 893–896.
- Treacy, M.M.J.; Ebbesen, T.W. & Gibson, J.M. (1996). Exceptionally high Young's modulus observed for individual carbon nanotubes. *Nature*, Vol. 381, pp. 678–680.

- Wang, X.; Padture, N.P. & Tanaka, H. (2004). Contact-damage-resistant ceramic/single-wall carbon nanotubes and ceramic/graphite composites. *Nature Materials*, Vol. 3, pp. 539-544.
- Yamamoto, G.; Omori, M.; Yokomizo, K.; Hashida, T. & Adachi, K. (2008). Structural characterization and frictional properties of carbon nanotube/alumina composites prepared by precursor method. *Materials Science and Engineering B*, Vol. 148, pp. 265–269.
- Yamamoto, G.; Omori, M.; Hashida, T. & Kimura, H. (2008). A novel structure for carbon nanotube reinforced alumina composites with improved mechanical properties. *Nanotechnology*, Vol. 19, article number: 315708.
- Yamamoto, G.; Omori, M.; Yokomizo, K. & Hashida, T. (2008). Mechanical properties and structural characterization of carbon nanotube/alumina composites prepared by precursor method. *Diamond and Related Materials*, Vol. 17, pp. 1554-1557.
- Yamamoto, G.; Suk, J.W.; An, J.; Piner, R.D.; Hashida, T.; Takagi, T. & Ruoff, R.S. (2010). The influence of nanoscale defects on the fracture of multi-walled carbon nanotubes under tensile loading. *Diamond and Related Materials*, Vol. 19, pp. 748-751.
- Yamamoto, G.; Shirasu, K.; Hashida, T.; Takagi, T.; Suk, J.W.; An, J.; Piner, R.D. & Ruoff, R.S. (2011). Nanotube fracture during the failure of carbon nanotube/alumina composites. *Carbon*, Vol. 49, pp. 3709-3716.
- Yao, W.; Liu, J.; Holland, T.B.; Huang, L.; Xiong, Y.; Schoenung, J.M. & Mukherjee, A.K. (2011). Grain size dependence of fracture toughness for fine grained alumina, *Scripta Materialia*, Vol. 65, pp. 143–146.
- Yu, M.F.; Lourie, O.; Dyer, M.J.; Moloni, K.; Kelly, T.F. & Ruoff, R.S. (2000). Strength and breaking mechanism of multiwalled carbon nanotubes under tensile load. *Science*, Vol. 287, pp. 637-640.
- Zhan, G.D.; Kuntz, J.D.; Wan, J. & Mukherjee, A.K. (2003). Single-wall carbon nanotubes as attractive toughening agents in alumina-based nanocomposites. *Nature Materials*, Vol. 2, pp. 38-42.